Composites Communications 25 (2021) 100703

Contents lists available at ScienceDirect

Composites Communications

journal homepage: www.elsevier.com/locate/coco

Pd–SnO_2 heterojunction catalysts anchored on graphene sheets for enhanced oxygen reduction

Guojie Chao [a], Longsheng Zhang [b], Jing Tian [a], Wei Fan [a,*], Tianxi Liu [a,b]

[a] State Key Laboratory for Modification of Chemical Fibers and Polymer Materials College of Materials Science and Engineering, Donghua University, Shanghai, 201620, PR China

[b] School of Chemical and Material Engineering, International Joint Research Laboratory for Nano Energy Composites, Jiangnan University, Wuxi, 214122, PR China

ARTICLE INFO

Keywords:
Electrocatalyst
Oxygen reduction reaction
Metal-support interaction
Zn-air battery

ABSTRACT

Palladium (Pd) has received extensive attention as the substitute for platinum to work as efficient catalyst towards the oxygen reduction reaction (ORR) owing to its high intrinsic activity. However, the Pd catalyst usually performs inferior catalytic stability in the practical electrochemical test. Here, we report a novel design of constructing efficient ORR catalyst with Pd/SnO_2 heterojunctions uniformly loaded on the reduced graphene oxide sheets (Pd@SnO_2/rGO). The highly conductive rGO sheets are beneficial to increase the electron transfers during the ORR process and the SnO_2 support can induce tensile-strain and electron-rich features for Pd nanocrystals in the Pd/SnO_2 heterojunctions. The electrochemical results illustrate that the Pd@SnO_2/rGO catalyst has higher ORR activity compared to commercial Pd/C and shows remarkable catalytic stability with 1 mV of negative shift in half-wave potential over 20000 cycles of accelerated durability tests. Moreover, the Zn-air battery assembled with Pd@SnO_2/rGO cathode exhibits a 2.8-fold higher specific capacity than that with Pd/C cathode.

1. Introduction

The metal-air batteries have been extensively researched as the promising energy conversion devices for their carbon-free emissions and high theoretical energy densities [1–5]. As the cathodic reaction for these applications, the electrocatalytic oxygen reduction reaction (ORR) suffers from sluggish reaction kinetics, limiting the overall energy conversion efficiency [6–9]. Currently, Pt-based materials can be excellent ORR catalysts due to their remarkable ORR activities. However, the high-price and scarce features of Pt limit the further advancement of Pt-based catalysts [10–13]. Preparing high-efficiency Pt-free ORR catalysts is significative for the development of metal-air batteries.

Among various alternative materials, the palladium (Pd) with similar electronic structure to Pt has higher intrinsic activity yet lower cost than -Pt [14–16]. Nevertheless, Pd-based catalysts also suffer from inferior catalytic durability towards ORR catalysis, which can be attributed to their strong adsorption of intermediates during the ORR process [17]. Great efforts have been reported to enhance the ORR performance of Pd-based catalysts by tuning their electronic structures, including strategies of composition control and doping with additional transition metals [18–20].

As reported, alloying Pd with other metals is a very effective strategy to boost the catalytic activity of Pd-based catalysts [21–23]. Unfortunately, owing to the inevitable dealloying and dissolution of metal dopants, the above strategies are unable to effectively improve the catalytic durability of Pd-based catalysts in spite of the enhanced ORR activities [24,25]. Subsequently, it is found that the ORR performance of Pd catalyst can be increased by loading Pd nanoparticles (NPs) on some carbon supports, like GO, CNT and porous carbon [26–28]. Especially, the N element doped carbon supports have been proved to be effective for boosting the catalytic performance of Pd catalyst [29]. However, the carbon materials are suffered from poor stability in the oxidative electrochemical environment [30], which causes the unsatisfied durabilities of Pd-based catalysts with carbon supports. Therefore, it is urgently desired to develop effective methodology for enhancing the catalytic stability of Pd-based catalysts towards ORR catalysis.

Recently, the metallic oxides are reported as the optimized catalyst supports to enhance the catalytic activities and stability of noble-metal electrocatalysts by strong metal-support interactions (SMSIs) [31–38]. The metal-oxide supports can adjust the electronic structures of the supported metal catalysts, which is beneficial to adjust the adsorption energies of intermediates [39–42]. Especially, the SnO_2 is reported as

* Corresponding author.
E-mail address: weifan@dhu.edu.cn (W. Fan).

https://doi.org/10.1016/j.coco.2021.100703
Received 16 January 2021; Received in revised form 1 March 2021; Accepted 1 March 2021
Available online 14 March 2021

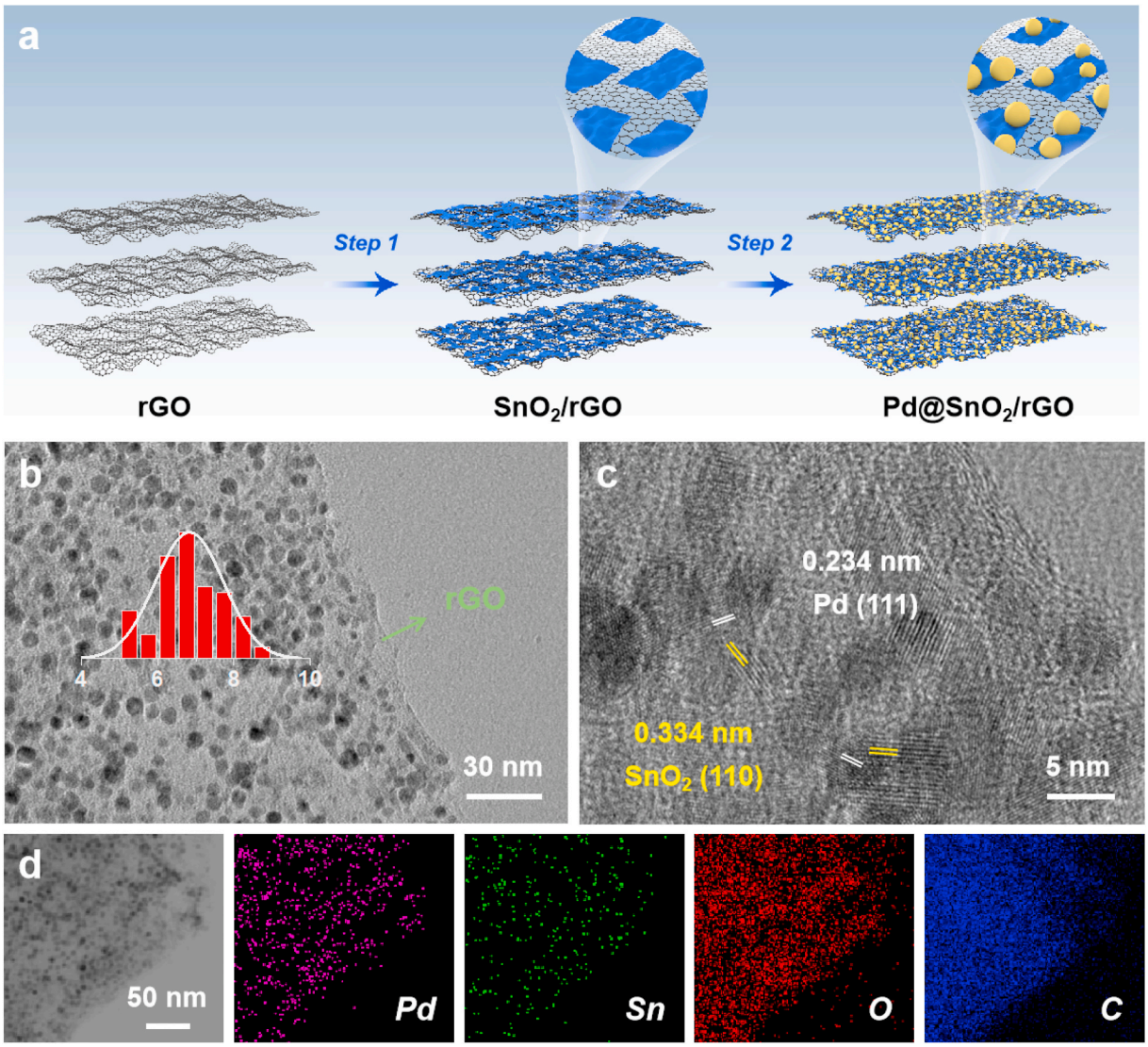

Fig. 1. (a) Schematic of the preparation process of Pd@SnO_2/rGO catalyst. (b, c) TEM images of Pd@SnO_2/rGO catalyst. (d) TEM and the corresponding elemental mapping images of Pd@SnO_2/rGO sample.

the good catalyst support for the characters of low price and excellent electrochemical durability [43,44]. Besides, the SnO_2 support can facilitate the desorption of unfavorable oxygen-containing intermediates on the active metal sites, thus enhancing the ORR performance of catalysts [45–47]. However, the electrical conductivity of SnO_2 support is relatively low, limiting the electron transfers during the electrochemical reaction process. To address these problems, we posit that constructing nanocomposites with Pd/SnO_2 heterojunctions supported onto conductive graphene sheets may function as efficient ORR catalysts with high activities and stability.

In this work, we propose a well-designed strategy of synthesizing efficient ORR catalysts with Pd@SnO_2 heterojunctions supported on reduced graphene oxide sheets (Pd@SnO_2/rGO). The heterojunction nanostructures can induce strong metal-support interactions by enabling large contact area between the Pd crystals and SnO_2 supports. The highly-conductive rGO sheets can not only prevent the aggregation of Pd@SnO_2 heterojunctions, but also increase the reaction kinetics by facilitating the electron transfers during the ORR process. We find that the SnO_2/rGO supports can induce lattice tensile strains and increase the electron densities of Pd nanocrystals. Such tensile-strain and electron-rich characters are not proved in the Pd nanocrystals supported on the carbon substrate (Pd/C), indicating the significant role of SMSIs. The Pd@SnO_2/rGO catalyst has enhanced catalytic activity toward ORR and exhibits excellent catalytic stability with 1 mV of negative shift in half-wave potential over 20000 cycles of accelerated durability tests, much lower than that (29 mV) of commercial Pd/C. Moreover, the Zn-air battery assembled with Pd@SnO_2/rGO cathode shows a 2.8-fold improvement in specific capacity compared to that with Pd/C cathode.

2. Experimental section

2.1. Preparation of SnO_2/rGO support

GO was first obtained using the Hummers' method [48,49]. Then, the SnO_2/rGO was synthesized according to the report [50]. Under stirring, the 40 mg of GO and 199 μL of $SnCl_4$ were dispersed into the solvent of oleic acid (20 mL), oleylamine (2.5 mL) and 10 mL methanol. After 1 h of ultrasound treatment, the mixed solution was transferred into the Teflon autoclave and then held at 180 °C for 18 h. Then, the black product was centrifuged and washed with ethanol for about 5 times. Finally, the product was dried in vacuum overnight.

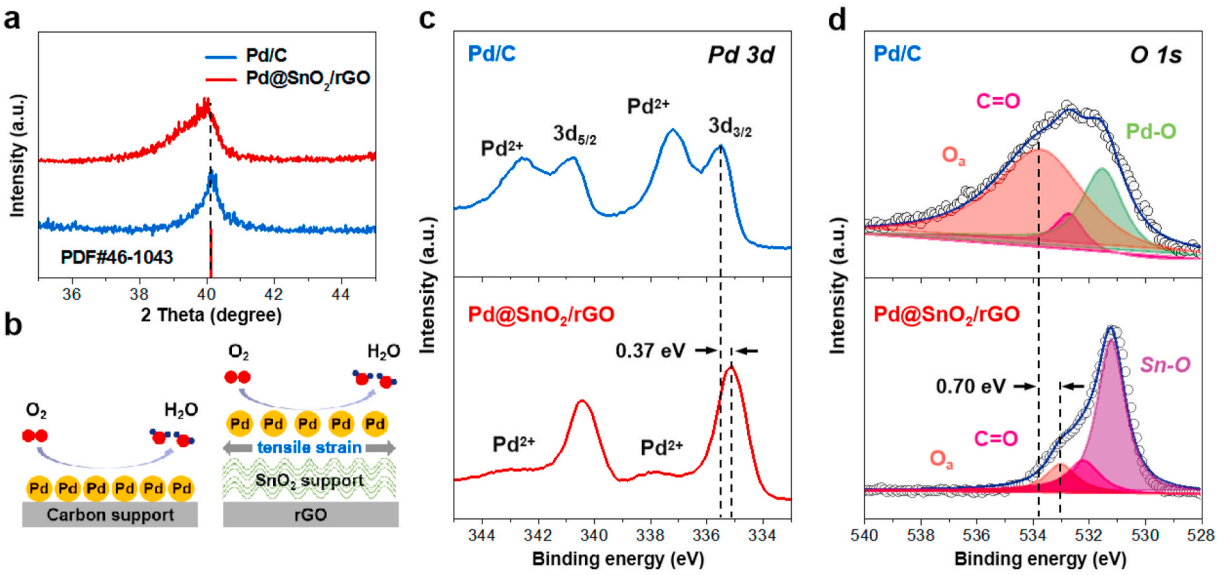

Fig. 2. (a) XRD patterns of Pd/C and Pd@SnO_2/rGO samples. (b) Schematic of the generated lattice tensile strains of Pd nanocrystals in the Pd@SnO_2/rGO catalyst. (c, d) High-resolution XPS spectra (Pd 3d and O 1s) of the Pd/C and Pd@SnO_2/rGO catalysts, respectively.

2.2. Preparation of Pd@SnO_2/rGO sample

The 40 mg of as-prepared SnO_2/rGO sample was dispersed in 30 mL of ethylene glycol under stirring. Next, Na_2PdCl_4 solution and PVP solution were prepared by dissolving 420 mg of PVP and 160 mg Na_2PdCl_4 into 3 mL of ethylene glycol, respectively. Then, Na_2PdCl_4 solution and PVP solution were slowly dropped into the dispersion solution of SnO_2/rGO at 160 °C. After 1 h of solvothermal treatment at 160 °C, the as-obtained product was centrifuged and washed with ethanol for about 5 times and dried in vacuum at 60 °C for overnight.

3. Results and discussion

As illustrated in Fig. 1a, the Pd@SnO_2/rGO composite was obtained by one sample approach using hydrothermal and solvothermal methods (see details in Experimental Section). With high surface areas and electrical conductivity, the rGO sheets can prevent the agglomeration of SnO_2 for effective material utilization and facilitate electron transfer during the test. Notably, the Pd@SnO_2 heterojunction nanostructures can induce strong metal-support interactions by enabling large contact area between Pd nanocrystals and SnO_2 supports. Fig. S1 is the XRD pattern of Pd@SnO_2/rGO, which demonstrates that the characteristic diffraction peaks are ascribed to the tetragonal phase SnO_2 and the metallic Pd in the face-centered cubic phase. Notably, there is none diffraction peaks of Pd-based alloy in the XRD pattern of Pd@SnO_2/rGO sample, which demonstrates that the presence of SnO_2 has no effect on the crystal form of Pd metallic. The XRD results illustrate that the Pd@SnO_2/rGO sample is successfully prepared. Moreover, the content of Pd elements in the Pd@SnO_2/rGO was test by using ICP-MS measurements. The result shows that weight percentage of Pd is ~10% in the Pd@SnO_2/rGO sample. The SEM and TEM images reveal the uniform distribution of Pd NPs on the SnO_2/rGO support with diameters of 5–7 nm (Fig. 1b and Fig. S2). In the high-resolution TEM image of Pd@SnO_2/rGO sample (Fig. 1c), it is illustrated that the (110) crystal plane of SnO_2 and the (111) crystal plane of Pd. Especially, the lattice spacing of Pd nanocrystals in Pd@SnO_2/rGO sample is 0.234 nm, which is 4% larger than that (0.225 nm) of Pd nanocrystals in commercial Pd/C (Fig. S3), suggesting the tensile strains generated in the Pd nanocrystals on the SnO_2/rGO support. Meanwhile, it is also observed that the Pd, Sn, C and O elements are homogeneously distributed in the TEM and corresponding EDS mapping images of Pd@SnO_2/rGO sample (Fig. 1d).

To further investigate the tensile strains of Pd NPs with respect to the effect of catalyst supports, comparative XRD studies were further carried out for the Pd/C and Pd@SnO_2/rGO materials. As shown in Fig. 2a and S4, the characteristic peak at ~40.1° in the XRD pattern of Pd@SnO_2/rGO material slightly shifted to smaller diffraction angle, compared to that of commercial Pd/C material. These results also verify the lattice-tensile features in the Pd NPs of Pd@SnO_2/rGO catalyst, which can be ascribed to the SMSIs between Pd NPs and SnO_2 supports (Fig. 2b). As reported, the tensile strains of Pd NPs would lower the adsorption energies of intermediates and improve their reaction rate towards ORR catalysis [17,20,51], which demonstrates that the supported Pd NPs on SnO_2 supports are promising to obtain the improved catalytic performance. Furthermore, the Raman spectra were also employed to evaluate the electrical conductivity of the carbon substrate of Pd@SnO_2/rGO and Pd/C samples. There are two peaks in the Raman spectra of Pd@SnO_2/rGO and Pd/C samples (Fig. S5), which are assigned as the peaks of G band (1587 cm^{-1}) and D band (1345 cm^{-1}), respectively. The ratio of intensity (I_D/I_G) is one important parameter to assess the degree of graphitization of the carbon substrates. The calculation results of I_D/I_G suggest that the successful reduction of GO sheets and the rGO substrate possess higher electrical conductivity for the smaller I_D/I_G. The Raman results illustrate that the rGO substrate can facilitate the electron transfer and provide faster reaction kinetics during the electrochemical reaction process.

We also conducted XPS measurements to research the chemical state of samples. In the XPS spectra of Pd@SnO_2/rGO and Pd/C samples (Fig. S6), it is clearly observed the characteristic peaks of Pd element. Notably, there are two prominent peaks in the Pd 3d spectra of Pd/C and Pd@SnO_2/rGO samples (Fig. 2c), which can be labeled as the Pd $3d_{3/2}$ peak and Pd $3d_{5/2}$ peak of metallic Pd (Pd^0). Moreover, there are two extra peaks in the Pd 3d spectra of these two samples, which can be ascribed to the presence of Pd–O species (Pd^{2+}) [19,52,53]. Besides, the percentage of Pd^0 species in Pd@SnO_2/rGO sample is much larger than that of Pd/C sample according to the XPS spectra. Especially, the XPS peak of Pd $3d_{3/2}$ for Pd@SnO_2/rGO has a downshift of 0.4 eV compared to the Pd/C sample. These results, taken together, indicate the increased electron densities of Pd crystals in the Pd@SnO_2/rGO sample. It can be ascribed to the charge transfers at the heterojunction interface of Pd crystals and SnO_2/rGO supports [46,54,55]. As reported, the electron-rich Pd sites can weaken the adsorption energies of oxygen species and thus enhance the catalytic stability [46,50,56]. As shown in

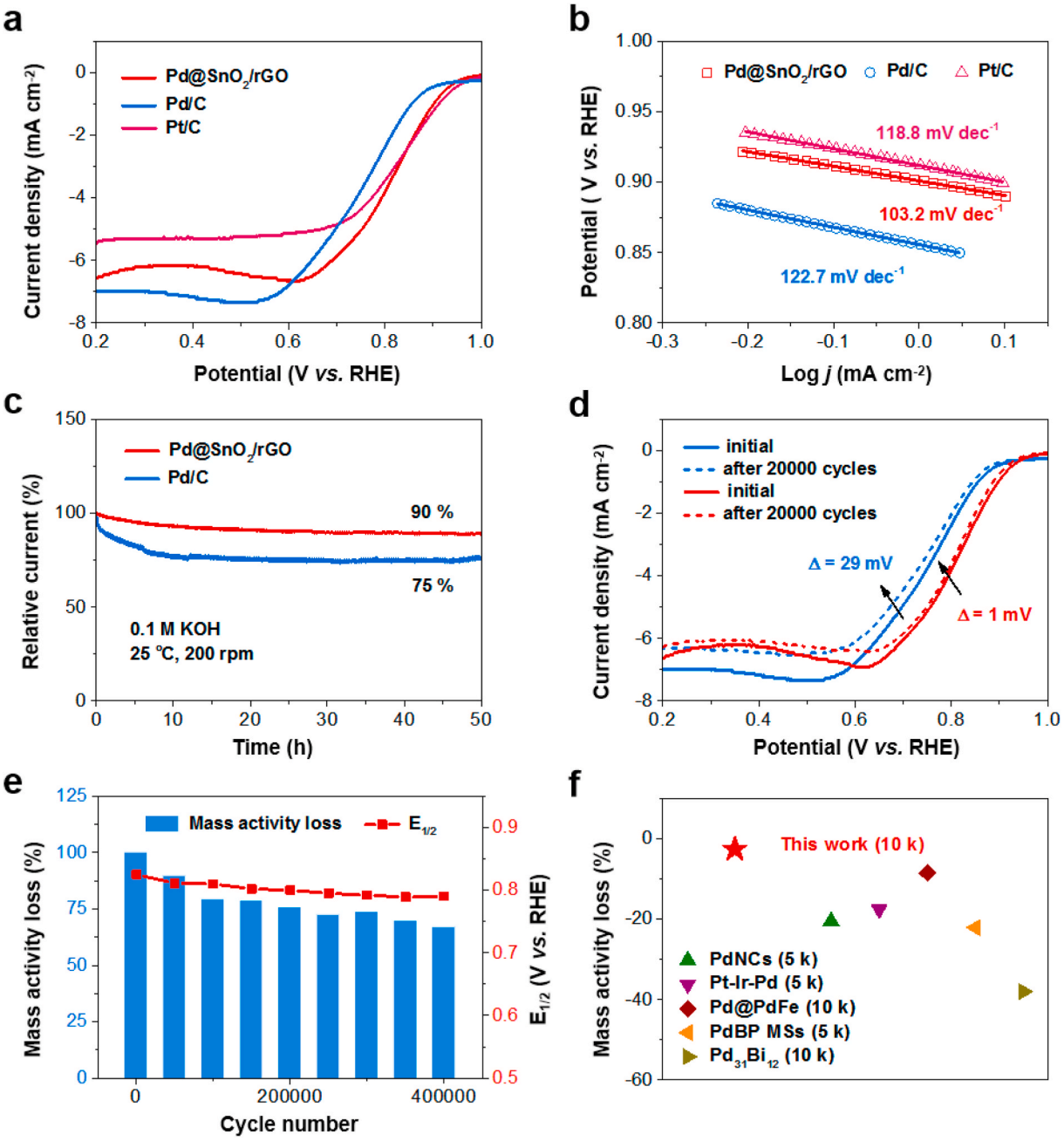

Fig. 3. (a, b) LSV curves and Tafel slopes of Pd@SnO_2/rGO, Pt/C and Pd/C catalysts, respectively. (c) Current-time chronoamperometric curves and (d) polarization curves of Pd@SnO_2/rGO and Pd/C catalysts. (e) Mass activity loss and half-wave potential ($E_{1/2}$) of Pd@SnO_2/rGO catalyst after different cycles of tests. (f) Comparison of the catalytic stabilities between the Pd@SnO_2/rGO catalyst and other previously-reported ORR catalysts.

the O 1s spectra (Fig. 2d), there is a characteristic peak of Pd–O species in the Pd/C sample, while no such peak is observed in the Pd@SnO_2/rGO sample. Besides, the peak intensity of absorbed oxygen species (O_a) on the Pd/C sample is higher than that of the Pd@SnO_2/rGO sample. The binding energy of O_a peak for the Pd@SnO_2/rGO sample shows a downshift of 0.7 eV compared with that of the Pd/C material, which is caused for the electron-rich features of Pd crystals in the Pd/SnO_2 heterojunctions.

The electrochemical measurements were conducted to assess the ORR performance of the two Pd-based catalysts. Comparing with CV curve measured in the N_2-saturated electrolytes (Fig. S7), the CV curve of Pd@SnO_2/rGO catalyst has an extra reduction peak in the O_2-saturated electrolytes, which suggests that the catalytic ORR takes place. As shown in Fig. S8, comparing the onset potential of oxygen reduction peak in the CV curves of Pd@SnO_2/rGO and Pd/C catalyst, the Pd@SnO_2/rGO catalyst shows superb catalytic activity toward ORR for the more positive oxygen reduction peak, much higher than that of Pd/C catalysts. As displayed in Fig. 3a, the ORR catalytic activity was also evaluated by conducting linear sweep voltammetry (LSV) measurements. The LSV curve of Pd@SnO_2/rGO catalyst exhibits a high half-wave potential (0.830 V *vs.* RHE), much higher than that of commercial Pd/C (0.761 *vs.* RHE) and slightly lower than that of Pt/C catalyst (0.841 *vs.* RHE). Moreover, the mass activity of Pd@SnO_2/rGO catalyst is 0.040 A mg_{Pd}^{-1} measured at 0.9 V (*vs.* RHE), which is higher than those of Pd/C (0.018 A mg_{Pd}^{-1}) and Pt/C (0.025 A·mg_{Pt}^{-1}). Meanwhile, the Pd@SnO_2/rGO catalyst has a lower Tafel slope (103.2 mV dec^{-1}) than those of Pd/C (122.7 mV dec^{-1}) and Pt/C (118.8 mV dec^{-1}) (Fig. 3b). The electron transfer number and H_2O_2 yield of catalysts were also

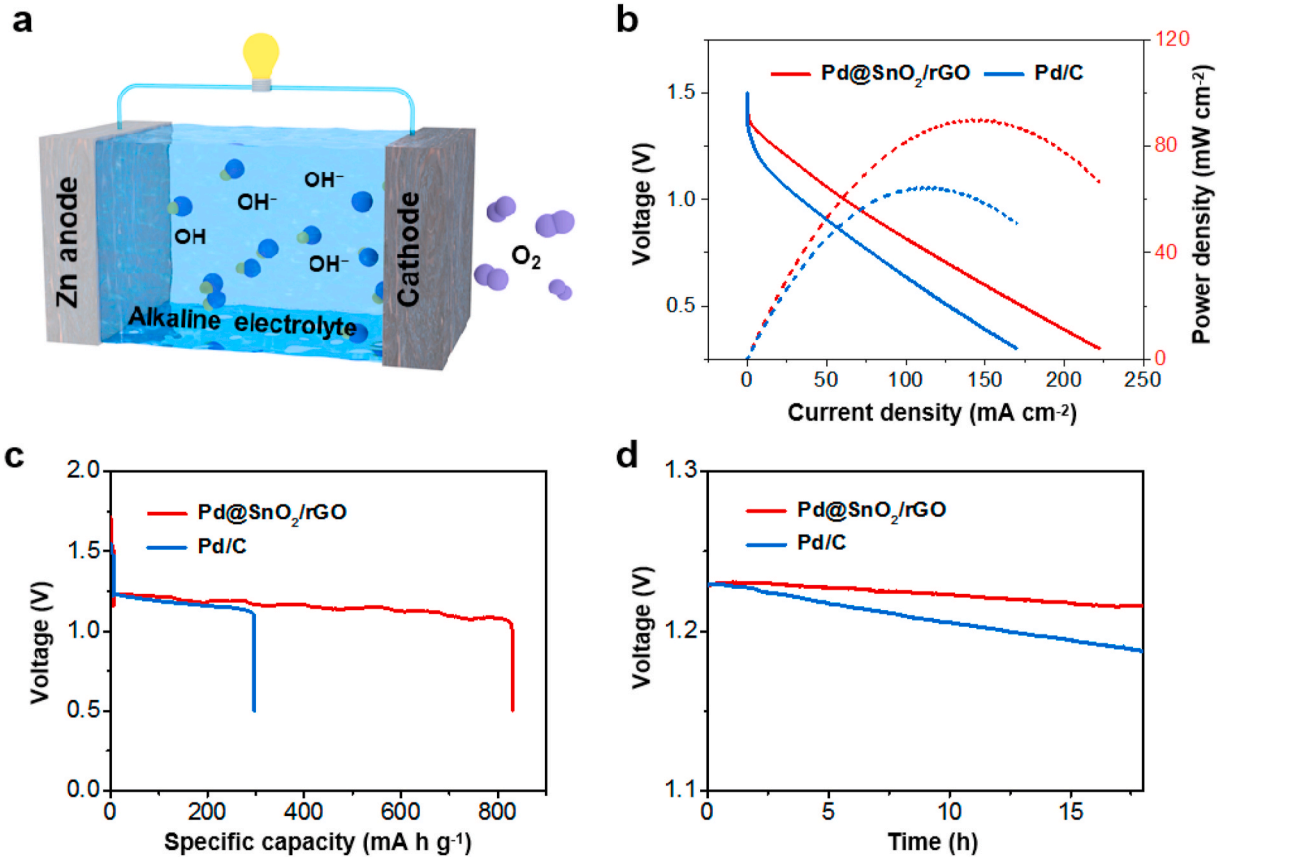

Fig. 4. (a) Schematic diagram of Zn-air battery. (b) Polarization curves and power densities of Zn-air batteries assembled with the Pd@SnO_2/rGO and Pd/C cathodes. (c, d) Specific capacities and galvanostatic discharge tests of Zn-air batteries using Pd@SnO_2/rGO and Pd/C cathodes, respectively.

measured by using the RRDE technique. According to the RRDE curves (Fig. S9), it is calculated that the electron transfer number of Pd@SnO_2/rGO catalyst is closer to 4 with low H_2O_2 yield (Fig. S10). In addition, the Pd@SnO_2/rGO catalyst exhibits superior methanol tolerance during the methanol toxicity test (Fig. S11).

The current-time chronoamperometric tests were further performed to verify the catalytic stability of catalysts. After 50 h test, the Pd@SnO_2/rGO catalyst shows a lower current attenuation of 10% in comparison with that (25%) of Pd/C catalyst (Fig. 3c). Furthermore, the accelerated durability tests were also conducted to check the catalytic durability of catalysts. After 20000 cycles of tests, the half-wave potential of Pd@SnO_2/rGO catalyst has a negative shift of 1 mV, which is greatly lower than that (29 mV) of Pd/C catalyst (Fig. 3d). Even after 400000 cycles of tests, the half-wave potential of Pd@SnO_2/rGO catalyst shows a negative shift of 34 mV (Fig. 3e and S12). The catalytic stability of Pd@SnO_2/rGO catalyst outperforms those of reported ORR catalysts (Fig. 3f and Table S1) [57–61]. Combining the TEM/XPS/XRD studies and electrochemical results, the generated tensile strains and increased electron densities of Pd nanocrystals in Pd@SnO_2/rGO catalyst contribute to its enhanced ORR activity and stability.

We next assembled a Zn-air battery using zinc foil as anode and Pd@SnO_2/rGO loaded onto commercial carbon paper as cathode in alkaline aqueous electrolyte (Fig. 4a). Notably, the Zn-air battery assembled with Pd@SnO_2/rGO cathode exhibits a power density of 90 mW cm^{-2} (Fig. 4b), which is higher than the battery assembled with the Pd/C cathode (63 mW cm^{-2}). Moreover, Fig. 4c shows that the battery with Pd@SnO_2/rGO cathode also has satisfactory specific capacity (832 mAh g^{-1}), while the battery with Pd/C cathode has only 297 mAh g^{-1} of specific capacity at the same current density. Moreover, the stability of Zn-air battery was conducted through galvanostatic discharge measurements. After 18 h of continuous operation, the Zn-air battery with Pd@SnO_2/rGO cathode has a low voltage loss of 11 mV, while the battery with Pd/C cathode suffers from rapid voltage decay of 42 mV (Fig. 4d). The Pd@SnO_2/rGO material as the high activity and durability catalyst shows great potential for its applications as cathodes in Zn-air batteries.

4. Conclusions

In conclusion, we demonstrate a novel design of efficient ORR catalysts with Pd@SnO_2 heterojunctions loaded on conductive graphene sheets, and the resultant Pd@SnO_2/rGO catalyst has excellent catalytic activity and durability to benchmark Pd/C catalyst. The TEM, XRD and XPS studies reveal that the SnO_2 catalyst supports can induce tensile-strain and electron-rich features of Pd nanocrystals in the Pd@SnO_2/rGO catalyst, while these features can not be observed in the Pd nanocrystals with carbon support in commercial Pd/C catalyst. The Pd@SnO_2/rGO catalyst exhibits satisfactory catalytic activity and stability toward ORR. Moreover, the Zn-air battery assembled with Pd@SnO_2/rGO cathode shows higher specific capacity and better cycling durability than that with Pd/C cathode. This work suggests that introducing optimal supports is an effective approach to prepare high-performance heterogeneous catalysts for electrochemical reactions.

CRediT authorship contribution statement

Guojie Chao: Methodology, Data processing, Writing – original draft. **Longsheng Zhang:** Conceptualization, Writing – review & editing. **Jing Tian:** Investigation. **Wei Fan:** Funding acquisition, Writing – review & editing, Supervision. **Tianxi Liu:** Funding acquisition, Writing – review & editing.

Declaration of competing interest

The authors declare that they have no known competing financial interests or personal relationships that could have appeared to influence the work reported in this paper.

Acknowledgements

The authors are grateful for the financial support from the National Natural Science Foundation of China (21875033, 21704014), the Fundamental Research Funds for the Central Universities (2232019A3-03), Shanghai Scientific and Technological Innovation Project (18JC1410600).

Appendix A. Supplementary data

Supplementary data to this article can be found online at https://doi.org/10.1016/j.coco.2021.100703.

References

[1] T.M. Gur, A. Heinzel, Review of electrical energy storage technologies, materials and systems: challenges and prospects for large-scale grid storage, Energy Environ. Sci. 11 (2018) 2696–2767.
[2] J. Han, X. Meng, L. Lu, J. Bian, Z. Li, C. Sun, Single-Atom Fe-N-x-C as an efficient electrocatalyst for zinc-air batteries, Adv. Funct. Mater. 29 (2019), 1808872.
[3] D.Y. Chung, J.M. Yoo, Y.E. Sung, Highly durable and active Pt-based nanoscale design for fuel-cell oxygen-reduction electrocatalysts, Adv. Mater. 30 (2018), 1704123.
[4] G. Chao, L. Zhang, D. Wang, S. Chen, H. Guo, K. Xu, W. Fan, T. Liu, Activation of graphitic nitrogen sites for boosting oxygen reduction, Carbon 159 (2020) 611–616.
[5] S. Yang, Y. Yu, M. Dou, Z. Zhang, F. Wang, Edge-functionalized polyphthalocyanine networks with high oxygen reduction reaction activity, J. Am. Chem. Soc. 142 (2020) 17524–17530.
[6] M. Li, Z. Zhao, T. Cheng, A. Fortunelli, C.Y. Chen, R. Yu, Q. Zhang, L. Gu, B. V. Merinov, Z. Lin, E. Zhu, T. Yu, Q. Jia, J. Guo, L. Zhang, W.A. Goddard, Y. Huang, X. Duan, Ultrafine jagged platinum nanowires enable ultrahigh mass activity for the oxygen reduction reaction, Science 354 (2016) 1414–1419.
[7] H. Guo, Q. Feng, K. Xu, J. Xu, J. Zhu, C. Zhang, T. Liu, Self-templated conversion of metallogel into heterostructured TMP@carbon quasiaerogels boosting bifunctional electrocatalysis, Adv. Funct. Mater. 29 (2019), 1903660.
[8] Y. Yuan, J. Wang, S. Adimi, H. Shen, T. Thomas, R. Ma, J.P. Attfield, M. Yang, Zirconium nitride catalysts surpass platinum for oxygen reduction, Nat. Mater. 19 (2020) 282–286.
[9] D. Li, H. Xu, L. Jiao, H. Jiang, Metal-organic frameworks for catalysis: state of the art, challenges, and opportunities, EnergyChem 1 (2019), 100005.
[10] Y. Liang, Y. Li, H. Wang, J. Zhou, J. Wang, T. Regier, H. Dai, Co_3O_4 nananonacrystals on graphene as a synergistic catalyst for oxygen reduction reaction, Nat. Mater. 10 (2011) 780–786.
[11] X. Wang, M.T. Swihart, G. Wu, Achievements, challenges and perspectives on cathode catalysts in proton exchange membrane fuel cells for transportation, Nat. Catal. 2 (2019) 578–589.
[12] T. Zhu, Q. Feng, S. Liu, C. Zhang, Metallogel-derived 3D porous carbon nanosheet composites as an electrocatalyst for oxygen reduction reaction, Compos. Commun. 20 (2020) 100376.
[13] Y. Chen, T. Cheng, W.A. Goddard, Atomistic explanation of the dramatically improved oxygen reduction reaction of jagged platinum nanowires, 50 times better than Pt, J. Am. Chem. Soc. 142 (2020) 8625–8632.
[14] E. Antolini, Palladium in fuel cell catalysis, Energy Environ. Sci. 2 (2009) 915–931.
[15] G. Bampos, L. Sygellou, S. Bebelis, Oxygen reduction reaction activity of Pd-based bimetallic electrocatalysts in alkaline medium, Catal. Today 355 (2020) 685–697.
[16] J. Jiang, W. Ding, W. Li, Z. Wei, Freestanding single-atom-Layer Pd-based catalysts: oriented splitting of energy bands for unique stability and activity, Inside Chem. 6 (2020) 431–447.
[17] L. Wang, Z. Zeng, W. Gao, T. Maxson, D. Raciti, M. Giroux, X. Pan, C. Wang, J. Greeley, Tunable intrinsic strain in two-dimensional transition metal electrocatalysts, Science 363 (2019) 870–874.
[18] J. Lin, C. Xi, Z. Li, Y. Feng, D. Wu, C. Dong, P. Yao, H. Liu, X. Du, Lattice-strained palladium nanoparticles as active catalyst for oxygen reduction reaction, Chem. Commun. 55 (2019) 3121–3123.
[19] M. Luo, Z. Zhao, Y. Zhang, Y. Sun, Y. Xing, F. Lv, Y. Yang, X. Zhang, S. Hwang, Y. Qin, J.-Y. Ma, F. Lin, D. Su, G. Lu, S. Guo, PdMo bimetallene for oxygen reduction catalysis, Nature 574 (2019) 81–85.
[20] Y. Shen, D. Shi, L. Liu, F. Liao, W. Zhu, M. Shao, Pd nanoparticles/F, N codoping graphene composites for oxygen reduction and zinc-air batteries, ACS Sustain. Chem. Eng. 7 (2019) 12281–12287.
[21] X. Jiang, K. Elouarzaki, Y. Tang, J. Zhou, G. Fu, J.-M. Lee, Embedded PdFe@N-carbon nanoframes for oxygen reduction in acidic fuel cells, Carbon 164 (2020) 369–377.
[22] G. Xu, C. Han, Y. Zhu, J. Zeng, J. Jiang, Y. Chen, PdCo alloy nanonetworks-polyallylamine inorganic-organic nanohybrids toward the oxygen reduction reaction, Adv. Mater. Interfaces (2018), 1701322.
[23] S. Huang, S. Lu, H. Hu, B. Cao, H. Li, F. Duan, H. Zhu, H. Gu, M. Du, A stable PdCu@Pd core-shell nanobranches with enhanced activity and methanol-tolerant for oxygen reduction reaction, Electrochim. Acta 354 (2020) 136680.
[24] M. Asano, R. Kawamura, R. Sasakawa, N. Todoroki, T. Wadayama, Oxygen reduction reaction activity for strain-controlled Pt-based model alloy catalysts: surface strains and direct electronic effects induced by alloying elements, ACS Catal. 6 (2016) 5285–5289.
[25] M. Escudero-Escribano, P. Malacrida, M.H. Hansen, U.G. Vej-Hansen, A. Velazquez-Palenzuela, V. Tripkovic, J. Schiotz, J. Rossmeisl, I.E.L. Stephens, Tuning the activity of Pt alloy electrocatalysts by means of the lanthanide contraction, Science 352 (2016) 73–76.
[26] S. Kabir, A. Serov, A. Zadick, K. Artyushkova, P. Atanassov, Palladium nanoparticles supported on three-dimensional graphene nanosheets: superior cathode electrocatalysts, ChemElectroChem 3 (2016) 1655–1666.
[27] S. Li, T. Wang, H. Xue, X. Fan, J. He, In-situ preparation of Pd incorporated ordered mesoporous carbon as efficient electrocatalyst for oxygen reduction reaction, Electrochim. Acta 191 (2016) 355–363.
[28] C.P. Deming, R. Mercado, J.N. Lu, V. Gadiraju, M. Khan, S. Chen, Oxygen electroreduction catalyzed by palladium nanoparticles dupported on nitrogen-doped graphene quantum dots: impacts of nitrogen dopants, ACS Sustain. Chem. Eng. 4 (2016) 6580–6589.
[29] T. Bhowmik, M.K. Kundu, S. Barman, Highly active and durable Pd nanoparticles-porous graphitic carbon nitride composite for electrocatalytic oxygen reduction reaction, Int. J. Hydrogen Energy 41 (2016) 14768–14777.
[30] G. Wang, Y. Yang, D. Han, Y. Li, Oxygen defective metal oxides for energy conversion and storage, Nano Today 13 (2017) 23–39.
[31] J.H. Kim, S. Chang, Y.T. Kim, Compressive strain as the main origin of enhanced oxygen reduction reaction activity for Pt electrocatalysts on chromium-doped titania support, Appl. Catal., B 158 (2014) 112–118.
[32] L. Zhang, L. Wang, H. Lin, Y. Liu, J. Ye, Y. Wen, A. Chen, L. Wang, F. Ni, Z. Zhou, S. Sun, Y. Li, B. Zhang, H. Peng, A lattice-oxygen-involved reaction pathway to boost urea oxidation, Angew. Chem. Int. Ed. 58 (2019) 16820–16825.
[33] I. Jimenez-Morales, F. Haidar, S. Cavaliere, D. Jones, J. Roziere, Strong interaction between platinum nanoparticles and tantalum-doped tin oxide nanofibers and its activation and stabilization effects for oxygen reduction reaction, ACS Catal. 10 (2020) 10399–10411.
[34] Y. Li, Y. Xu, Y. Liu, H. Pang, Exposing {001} crystal plane on hexagonal Ni-MOF with surface-grown cross-linked mesh-structures for electrochemical energy storage, Small 15 (2019), 1902463.
[35] J. Li, W. Zhang, X. Zhang, L. Huo, J. Liang, L. Wu, Y. Liu, J. Gao, H. Pang, H. Xue, Copolymer derived micro/meso-porous carbon nanofibers with vacancy-type defects for high-performance supercapacitors, J. Mater. Chem. 8 (2020) 2463–2471.
[36] X. Li, Q. Zhu, MOF-based materials for photo- and electrocatalytic CO_2 reduction, EnergyChem 2 (2020) 100033.
[37] K.M. Naik, E. Higuchi, H. Inoue, Two-dimensional oxygen-deficient TiO_2 nanosheets-supported Pt nanoparticles as durable catalyst for oxygen reduction reaction in proton exchange membrane fuel cells, J. Power Sources 455 (2020) 227972.
[38] Y. Xue, S. Zheng, H. Xue, H. Pang, Metal-organic framework composites and their electrochemical applications, J. Mater. Chem. 7 (2019) 7301–7327.
[39] S.J. Tauster, S.C. Fung, R.T. Baker, J.A. Horsley, Strong interactions in supported-metal catalysts, Science 211 (1981) 1121–1125.
[40] J. Ftouni, A. Munoz-Murillo, A. Goryachev, J.P. Hofmann, E.J.M. Hensen, L. Lu, C. J. Kiely, P.C.A. Bruijnincx, B.M. Weckhuysen, ZrO_2 is preferred over TiO_2 as support for the Ru-catalyzed hydrogenation of levulinic acid to gamma-valerolactone, ACS Catal. 6 (2016) 5462–5472.
[41] F. Lai, W. Zong, G. He, Y. Xu, H. Huang, B. Weng, D. Rao, J.A. Martens, J. Hofkens, I.P. Parkin, T. Liu, N_2 electroreduction to NH_3 by selenium vacancy-rich $ReSe_2$ catalysis at an abrupt interface, Angew. Chem. Int. Ed. 59 (2020) 13320–13327.
[42] M. Ren, F. Chang, R. Miao, X. He, L. Yang, X. Wang, Z. Bai, Strained lattice platinum-palladium alloy nanowires for efficient electrocatalysis, Inorg. Chem. Front. 7 (2020) 1713–1718.
[43] P. Zhang, S. Huang, B.N. Popov, Mesoporous tin oxide as an oxidation-resistant catalyst support for proton exchange membrane fuel cells, J. Electrochem. Soc. 157 (2010) B1163–B1172.
[44] G. Cognard, G. Ozouf, C. Beauger, G. Berthome, D. Riassetto, L. Dubau, R. Chattot, M. Chatenet, F. Maillard, Benefits and limitations of Pt nanoparticles supported on highly porous antimony-doped tin dioxide aerogel as alternative cathode material for proton-exchange membrane fuel cells, Appl. Catal., B 201 (2017) 381–390.
[45] F.B. Ometto, E.A. Carbonio, E. Teixeira-Neto, H.M. Villullas, Changes induced by transition metal oxides in Pt nanoparticles unveil the effects of electronic properties on oxygen reduction activity, J. Mater. Chem. 7 (2019) 2075–2086.
[46] S. Hussain, N. Kongi, H. Erikson, M. Rahn, M. Merisalu, L. Matisen, P. Paiste, J. Aruvali, V. Sammelselg, L.A. Estudillo-Wong, K. Tammeveski, N. Alonso-Vante, Platinum nanoparticles photo-deposited on SnO_2-C composites: an active and durable electrocatalyst for the oxygen reduction reaction, Electrochim. Acta 316 (2019) 162–172.
[47] X. Shen, T. Nagai, F. Yang, L. Zhou, Y. Pan, L. Yao, D. Wu, Y. Liu, J. Feng, J. Guo, H. Jia, Z. Peng, Dual-site cascade oxygen reduction mechanism on SnOx/Pt-Cu-Ni for promoting reaction kinetics, J. Am. Chem. Soc. 141 (2019) 9463–9467.

[48] J. Chen, Y. Li, L. Huang, C. Li, G. Shi, High-yield preparation of graphene oxide from small graphite flakes via an improved Hummers method with a simple purification process, Carbon 81 (2015) 826–834.
[49] G. Zhao, J. Li, X. Ren, C. Chen, X. Wang, Few-layered graphene oxide nanosheets as superior sorbents for heavy metal ion pollution management, Environ. Sci. Technol. 45 (2011) 10454–10462.
[50] S. Liu, J. Xiao, X. Lu, J. Wang, X. Wang, X.W. Lou, Efficient electrochemical reduction of CO_2 to HCOOH over sub-2nm SnO_2 quantum wires with exposed grain boundaries, Angew. Chem. Int. Ed. 58 (2019) 8499–8503.
[51] W. Zhu, H. Yuan, F. Liao, Y. Shen, H. Shi, Y. Shi, L. Xu, M. Ma, M. Shao, Strain engineering for janus palladium-gold bimetallic nanoparticles: enhanced electrocatalytic performance for oxygen reduction reaction and zinc-air battery, Chem. Eng. J. 389 (2020) 124240.
[52] W. Jiao, C. Chen, W. You, J. Zhang, J. Liu, R. Che, Yolk-shell Fe/Fe_4N@Pd/C Magnetic Nanocomposite as an Efficient Recyclable ORR Electrocatalyst and SERS Substrate, 2019, 1805032. Small.
[53] W. Tamakloe, D.A. Agyeman, M. Park, J. Yang, Y.M. Kang, Polydopamine-induced surface functionalization of carbon nanofibers for Pd deposition enabling enhanced catalytic activity for the oxygen reduction and evolution reactions, J. Mater. Chem. 7 (2019) 7396–7405.
[54] J. Li, H. Zhou, H. Zhuo, Z. Wei, G. Zhuang, X. Zhong, S. Deng, X. Li, J. Wang, Oxygen vacancies on TiO_2 promoted the activity and stability of supported Pd nanoparticles for the oxygen reduction reaction, J. Mater. Chem. 6 (2018) 2264–2272.
[55] Y. Li, C. Zhou, H. Zhang, H. He, J. Zhang, M. Chen, Influence of alkali metals on Pd/TiO_2 catalysts for catalytic oxidation of formaldehyde at room temperature, Catal. Sci. Technol. 6 (2016) 2289–2295.
[56] C. Tang, N. Zhang, Y. Ji, Q. Shao, Y. Li, X. Xiao, X. Huang, Fully tensile strained Pd_3Pb/Pd tetragonal nanosheets enhance oxygen reduction catalysis, Nano Lett. 19 (2019) 1336–1342.
[57] L. Sahoo, U.K. Gautam, Boosting bifunctional oxygen reduction and methanol oxidation electrocatalytic activity with 2D superlattice-forming Pd nanocubes generated by precise acid etching, ACS Appl. Nano Mater. 3 (2020) 8117–8125.
[58] J. Zhu, M. Xie, Z. Chen, Z.H. Lyu, M.F. Chi, W. Jin, Y. Xia, Pt-Ir-Pd trimetallic nanocages as a dual catalyst for efficient oxygen reduction and evolution reactions in acidic media, Adv. Energy Mater. 10 (2020), 1904114.
[59] X. Li, X. Li, C. Liu, H. Huang, P. Gao, F. Ahmad, L. Luo, Y. Ye, Z. Geng, G. Wang, R. Si, C. Ma, J. Yang, J. Zeng, Atomic-level construction of tensile-strained PdFe alloy surface toward highly efficient oxygen reduction electrocatalysis, Nano Lett. 20 (2020) 1403–1409.
[60] H. Lv, D. Xu, L. Sun, J. Henzie, S.L. Suib, Y. Yamauchi, B. Liu, Ternary palladium-boron-phosphorus alloy mesoporous nanospheres for highly efficient electrocatalysis, ACS Nano 13 (2019) 12052–12061.
[61] Y. Wang, D. Sun, T. Chowdhury, J.S. Wagner, T.J. Kempa, A.S. Hall, Rapid room-temperature synthesis of a metastable ordered intermetallic electrocatalyst, J. Am. Chem. Soc. 141 (2019) 2342–2347.